

Astrophysical Journal, in press, 10 July 2006, v645n 2 issue.

The Importance of Phase in Nulling Interferometry and a Three Telescope Closure-Phase Nulling Interferometer Concept

W. C. Danchi, J. Rajagopal¹, M. Kuchner, J. Richardson, D. Deming²

NASA Goddard Space Flight Center, Exoplanets and Stellar Astrophysics Laboratory, Code 667, Greenbelt, MD 20771

William.C.Danchi@nasa.gov

ABSTRACT

We discuss the theory of the Bracewell nulling interferometer and explicitly demonstrate that the phase of the “white light” null fringe is the same as the phase of the bright output from an ordinary stellar interferometer. As a consequence a “closure phase” exists for a nulling interferometer with three or more telescopes. We calculate the phase offset as a function of baseline length for an Earth-like planet around the Sun at 10 pc, with a contrast ratio of 10^{-6} at 10 μm . The magnitude of the phase due to the planet is $\sim 10^{-6}$ radians, assuming the star is at the phase center of the array. Although this is small, this phase may be observable in a three-telescope nulling interferometer that measures the closure phase. We propose a simple non-redundant three-telescope nulling interferometer that can perform this measurement. This configuration is expected to have improved characteristics compared to other nulling interferometer concepts, such as a relaxation of pathlength tolerances, through the use of the “ratio of wavelengths” technique, a closure phase, and better discrimination between exodiacal dust and planets.

Subject headings: telescopes — techniques: interferometric — techniques: high angular resolution — stars: planetary systems — stars: circumstellar material

¹University of Maryland, Astronomy Department, College Park, MD 20742

²Planetary Systems Laboratory, Code 693, Goddard Space Flight Center, Greenbelt, MD 20771

1. Introduction

Direct imaging of Earth-like planets around nearby stars is extremely difficult for two fundamental reasons. The first is the need for resolution well below one arcsec; the second is the extremely large contrast ratio between the planet and star, which is $\sim 10^{-6} - 10^{-7}$ at mid-infrared wavelengths (e.g., 5-20 μm) and $\sim 10^{-9} - 10^{-10}$ at visible wavelengths (400-900 nm). Generally, interferometric techniques are favored in the infrared, while coronagraphic techniques have received the most attention at visible wavelengths. The extrasolar zodiacal dust around these stars provides an additional complication, primarily because their intensity compared to the zodiacal dust in our own Solar system, and also their spatial distribution, is largely unknown.

Interferometric methods for direct detection of extrasolar planets are derived from the initial concept of Bracewell (1978) (see also Bracewell & MacPhee 1979) of a rotating two-telescope interferometer, in which a 180 degree phase shift was applied to the electric field from one of the two telescopes. The net result of this phase shift is a response pattern with a minimum or “null” response on-axis (zero pathlength difference between the two telescopes), which suppresses the unwanted signal from the starlight, and has a maximum response off-axis, at an angle proportional to the wavelength of light divided by the separation between the two telescopes.

More than a quarter century has passed since that initial paper, and there has been a substantial body of work in which a variety of array configurations of interferometers has been proposed for planet detection, including the OASES (Angel & Woolf 1997), Dual-Chopped Bracewell (Woolf et al. 1998), and Darwin (Leger et al. 1996, Mennesson & Marriotti 1997) configurations, respectively. These interferometers were designed to improve the response of the array, principally to reduce the effect of stellar leakage, such as in the OASES array, or to allow for subtraction of a symmetrical distribution of extrasolar zodiacal dust, as in the Dual-Chopped Bracewell array. Essentially all studies of the potential performance of these arrays have been based on calculations of the response of the array in the far-field in which the interferometers are viewed as a phased array, and only the intensity at the nulled output of the interferometer is considered (e.g., as described in Mennesson & Marriotti 1997).

However, the literature on nulling interferometry has not been explicitly connected to the large body of work on conventional optical interferometers (in which the inputs from the individual elements are combined in phase at zero pathlength difference). In particular, the observable quantity called the “closure phase,” was originally developed by Jennison (1958) for phase-unstable radio interferometers, and has been used successfully at visible and infrared wavelengths in the past few years. For example, images of complex sources, such as the surfaces of stars (Young et al. 2000), and clumpy, dusty outflows around massive

stars like the spiral-shaped outflow discovered around WR 104 (Tuthill, Monnier, & Danchi 1999), have been synthesized at very high angular resolution (i.e., $\ll 0.1$ arcsec), at visible and infrared wavelengths, respectively, using this technique.

In this paper we examine the fundamental connection between nulling interferometers and conventional stellar interferometers. We begin by showing that the phase of the “white light” null fringe is the same as that of the “white light” bright fringe from an ordinary stellar interferometer. For two sources with very unequal intensities, such as a star and an earth-like planet, we show that the phase is small but is observable. We demonstrate the existence of a “closure phase” for nulling interferometers. Finally, we propose a simplified non-redundant three-telescope nulling interferometer for the detection of Earth-like planets, which includes a “null” closure phase. This configuration is expected to have improved characteristics including essentially no variability noise, a relaxation of pathlength tolerances through the use of the “ratio of wavelengths” technique and a closure phase.

2. The Phase of the Null Fringe

Figure 1 displays a typical experimental situation for a simplified two-telescope nulling interferometer. Let E_1 be the electric field at the location \mathbf{r} , and E_2 be the complex electric field at the location $\mathbf{r} + \mathbf{B}$, where \mathbf{B} is the baseline vector separating the centers of the two telescopes (e.g., the central ray in geometric optics), and $\mathbf{r} = (x, y, z)$ and $\mathbf{B} = (B_x, B_y, B_z)$, are the cartesian coordinates of the position vector of the center of the first telescope, and the baseline vector, respectively. An achromatic π phase shift is applied to the electric field E_1 , and the two fields are combined on an ideal 50% beamsplitter labeled BS in the figure. The intensities measured at the two output ports of the beamsplitter are labeled I_1 and I_2 , respectively. The time averaged correlation between the two electric fields is given by:

$$\tilde{\Gamma}_{12} = \langle E_1(\mathbf{r}, t) E_2^*(\mathbf{r} + \mathbf{B}, t) \rangle \quad (1)$$

By the van Cittert-Zernike theorem of optics (see Thompson, Moran, and Swenson 2001) the quantity $\tilde{\Gamma}_{12}$ is proportional to the complex visibility¹ of the source intensity distribution in the far field of the array. Thus, we can define $\tilde{\Gamma}_{12} \equiv |\Gamma_{12}| e^{i\phi_{12}}$, where $|\Gamma_{12}|$ is the visibility amplitude and ϕ_{12} is the visibility phase.

We assume the electric fields from the two telescopes have additional phases ϕ_1 , and ϕ_2

¹ $\tilde{\Gamma}_{12}$ is the “mutual intensity function” (Goodman 1985), which when normalized by the total flux leads to the “complex coherence factor.” By the van Cittert-Zernike theorem (Thompson, Moran, & Swenson 2001) this is the Fourier transform of the object intensity and is the classical visibility when $I_1 = I_2$.

before they are combined at the beamsplitter, such as might be due to pathlength variations or mismatches between the two arms of the array. By expanding Eqn. (1) the resultant intensities are (in units where $c/8\pi = 1$):

$$I_1 = 1/2 [|E_1|^2 + |E_2|^2 - 2|\Gamma_{12}| \cos(\phi_{12} + \phi_1 - \phi_2)] \quad (2)$$

$$I_2 = 1/2 [|E_1|^2 + |E_2|^2 + 2|\Gamma_{12}| \cos(\phi_{12} + \phi_1 - \phi_2)] \quad (3)$$

where I_1 is the intensity at the null output port of the interferometer, and I_2 is the intensity at the bright output. If the output intensities are normalized to the total power incident on the array, i.e., by dividing I_1 and I_2 by $I_T = |E_1|^2 + |E_2|^2$ and defining the normalized visibility, $|V_{12}| = 2|\Gamma_{12}|/I_T$, then we can rewrite the above equations as:

$$\tilde{I}_1 = 1/2 [1 - |V_{12}| \cos(\phi_{12} + \phi_1 - \phi_2)] \quad (4)$$

$$\tilde{I}_2 = 1/2 [1 + |V_{12}| \cos(\phi_{12} + \phi_1 - \phi_2)] \quad (5)$$

where $\tilde{I}_1 = I_1/I_T$ and $\tilde{I}_2 = I_2/I_T$.

Thus we see that the phase terms for \tilde{I}_1 and \tilde{I}_2 are identical and both contain the same visibility phase, ϕ_{12} . This emphasizes the often overlooked fact that there is only one phase in any stellar interferometer.² The fact that the null output is “locked in” at the position of the star has dominated thinking in terms of current designs for the detection of earth-like planets around nearby stars, and as a result, phase measurements have not been considered (e.g., Angel & Woolf 1997). However, there is no fundamental obstacle to the measurement of the phase. For example, a ditherless quadrature phase detection scheme (see Barry et al. 2005) at the bright output or a small dither at the null output should suffice. In any case, some measurement of the null phase (measured by delay offsets) is necessary in order to locate and track the minimum intensity at the null output port relative to the delay set by the fringe tracking system, as in the design of the Fourier-Kelvin Stellar Interferometer (FKSI) (Danchi et al. 2003, 2004; Hyde et al. 2004). Furthermore, as shown in the next section, this phase is small but it can be measured and should not be ignored in the design of nulling interferometers for planet detection.

3. Understanding the Null Phase

Figure 2 displays a schematic diagram of the geometry of a binary system, e.g., a star and planet if the ratios of the two intensities, I_A , located at $(0,0)$ and I_B , at (x_0, y_0) , are

²Indeed, the complementary output from the pupil plane combiner of all conventional interferometers is a null by the conservation of energy, and this output is well established to have the same phase as the bright output.

large. The complex visibility is calculated by a simple Fourier transform of

$$I_T(x, y) = I_A \delta(x, y) + I_B \delta(x - x_0, y - y_0). \quad (6)$$

For the purpose of the present discussion we assume both sources are point sources. The visibility amplitude, $V(u, v)$, normalized to the total intensity, and phase, $\phi(u, v)$, are given by:

$$V(u, v) = \left[\frac{I_A^2 + I_B^2 + 2I_A I_B \cos 2\pi(ux_0 + vy_0)}{(I_A + I_B)^2} \right]^{1/2} \quad (7)$$

$$\phi(u, v) = -\arctan \left[\frac{I_B \sin 2\pi(ux_0 + vy_0)}{I_A + I_B \cos 2\pi(ux_0 + vy_0)} \right] \quad (8)$$

where (u, v) denotes the usual coordinates in the Fourier plane.

For simplicity, let us take a one-dimensional example. Let $y_0 = 0$, $u = B_0/\lambda$, and $I_A \gg I_B$. Let x_0 be the angular separation of the two point sources. With these assumptions, Eqn. (8) reduces to:

$$\phi \sim -\arctan [(I_B/I_A) \sin(2\pi B_0 x_0/\lambda)] \quad (9)$$

As a simple numerical example, assume $x_0 = 0.1$ arcsec and if $\lambda = 10 \mu\text{m}$, then the phase passes through zero when $2\pi B_0 x_0/\lambda = \pi$, i.e., when $x_0 = \lambda/2B_0$. This is exactly the same angular size given by the usual definition of resolution in conventional stellar interferometry, which is that two point sources are resolved if their separation $x_0 > \lambda/2B_0$, or for the parameters in this example, $x_0 > 0.05$ arcsec. The quantity $1 - V$ can be expanded, like the expression for the phase, ϕ , and is given by:

$$1 - V \sim (I_B/I_A)[1 - \cos(2\pi B_0 x_0/\lambda)]. \quad (10)$$

From this result, we see that the output of the nulling interferometer is essentially the intensity of the planet with the stellar flux removed. We also observe that $1 - V$ is maximized at $x_0 = \lambda/2B_0$, which is the same as the condition for the phase, ϕ , to pass through zero.

Figure 3(a) (upper panel) displays the null phase, ϕ , while Fig. 3(b) (lower panel) displays the normalized intensity, $1 - V$, of the null output port, i.e., from Eqn. (4), respectively. In this calculation we assume intensities, $I_B = 10^{-6}$, $I_A = 1 - I_B$, and baselines ranging from 0 to 40 m at $10 \mu\text{m}$, for an angular separation of 0.1 arcsec for the two sources (the Sun-Earth separation at 10 parsecs). We clearly see that the object phase varies and is of the order of 2×10^{-6} radians, or about 10^{-4} degrees. This is small but it can be measured, even with substantial pathlength fluctuations within the array, by the use of the closure phase concept, which we now discuss.

From Eqns. (2)-(5), we see that for a telescope pair, there is a phase term,

$$\tilde{\phi}_{12} = \phi_{12} + \phi_1 - \phi_2 \quad (11)$$

which is the object phase, ϕ_{12} , plus the telescope dependent phase errors, ϕ_1 and ϕ_2 , respectively. For a three-telescope nulling interferometer, shown schematically in Fig. 4 and described in the next section, there are equivalent expressions to Eqn. (8) for each telescope,

$$\tilde{\phi}_{23} = \phi_{23} + \phi_2 - \phi_3 \quad (12)$$

$$\tilde{\phi}_{13} = \phi_{13} + \phi_1 - \phi_3 \quad (13)$$

Adding Eqns. (11)-(13), it is easy to show there is a closure phase relation,

$$\phi_C = \tilde{\phi}_{12} + \tilde{\phi}_{23} - \tilde{\phi}_{13} \quad (14)$$

$$= \phi_{12} + \phi_{23} - \phi_{13} \quad (15)$$

which is exactly the same closure phase relation that is normally obtained in ground-based stellar interferometry.

From ground-based interferometry we know that the closure phase can be measured with good precision even in the presence of very large pathlength fluctuations in the atmosphere. For example, at the IOTA interferometer at Mt. Hopkins, closure phases are commonly measured to a precision of approximately 1 degree at 2 μm , for pathlength fluctuations on the order of 10 μm . Thus there is an effective suppression of the fluctuations by about a factor of 1800 (Ragland et al. 2004). Similar results have been obtained with the Infrared Spatial Interferometer at Mt. Wilson (Hale, Weiner, & Townes 2004).

For a stellar interferometer operated in space, we assume that the fringes are sensed and tracked at a wavelength of 2 μm . If the science band of the instrument is at 10 μm , and if the fringes are tracked to an RMS precision of 1 degree at 2 μm (i.e., 0.2 degrees at 10 μm), then in principle it should be possible to obtain an improvement in precision by using the closure phase at 10 μm to $\sim 0.2/1800 \approx 10^{-4}$. Thus, the closure phase technique can be used to obtain the precision required for the detection of Earth-like planets in the Solar neighborhood.

The fringe tracking precision quoted above is a very conservative one, and is based on assuming a very small collecting area of about 1 m^2 , i.e., a two-telescope interferometer like IOTA, consisting of 1/2 m in diameter telescopes. In principle it is possible to track the fringes to a much higher precision, as we show in the following calculation.

The rms error in determining the fringe phase is given by

$$\sigma_\phi = \sqrt{\frac{2}{NV^2}}, \quad (16)$$

where N is the number of photons collected, and V is the visibility of the fringe amplitude (Goodman 1985). Current designs for the Terrestrial Planet Finder Interferometer (TPF-I) mission envision much larger apertures, most likely in the 3-4 m diameter range (Beichmann, Woolf, & Lindensmith 1999). For a pair of such telescopes, the collecting area is 14-25 m². Assuming an optical efficiency of 10%, a bandwidth of 50% at a center wavelength of 2 μ m, and an integration time of 0.01 sec, we can easily estimate the attainable precision in tracking the fringe phase at 2 μ m. For a solar type star at 10 pc, it is easy to show that $N \sim (0.7 - 1.3) \times 10^7$ photons for this short integration time. Assuming $V \sim 1$, then the error in the phase measurement is $(1.6 - 2.0) \times 10^{-2}$ degrees. Thus the phase error due to tracking the fringes at 10 μ m is $(3 - 4) \times 10^{-3}$ degrees. This means the suppression required from the closure phase technique is only about a factor of 10-20, much less than the factor of 1800, which has been routinely achieved using current ground-based interferometers, like IOTA and ISI. We conclude that for a large space interferometer such as envisioned for TPF-I, only a modest suppression is needed from the closure phase technique.

In ground based radio interferometry, high dynamic range imaging is achieved through self-calibration and closure-phase calibration as described by Perley (1999). The technique of self-calibration, which is used to reduce antenna-based errors, employs a process of developing a model of a point source based on the data itself. The complex gains are computed from the point source model and then used to correct the visibilities. A new model is formed from the corrected visibilities and the process is repeated as necessary. Following this, a closure correction can be applied by additional measurements of strong point sources, and this additional calibration gives dynamic ranges as high as 10⁵. Part of the robustness of the closure phase technique in radio astronomy is due to the fact that there are a large number of antennas, e.g., 27 for the Very Large Array, which allows for many closure phases to be determined, as well as closure amplitudes (Pearson & Readhead 1984). This allows for recovery of most of the visibility phase and amplitude information from the closure amplitude and phases.

However, phase closure techniques are limited in part by baseline-based errors, which are not calibrated out between source and calibrator measurements (see Perley 1999, and references therein). Baseline dependent errors include correlator errors that cause non-factorable gain errors (e.g., Cornwell & Fomalont 1999), but these errors can be made negligible using the best current correlator designs. The accuracy and stability of the baseline measurements affects the dynamic range as well, as baseline variations that occur between source and calibrator measurements will not be removed.

For structurally connected space-based infrared interferometers for planet detection will use passive cooling (e.g., using a sunshade) to reduce thermal noise, and with careful design,

thermal drifts which could affect the baseline length due to motion between source and calibrator can be substantially less than a degree. Composite structures also can have extremely small thermal expansion coefficients at the instrument temperature (expected to be around 35 K).

Free-flying space based interferometers are more similar in nature to ground-based interferometers because of baseline drifts. In space these are likely due to imperfect formation control, however, metrology systems can be employed to retain knowledge of the baselines to a very high precision, i.e., much less than $1 \mu\text{m}$, consequently this source of closure phase errors can be substantially reduced through calibration. In ground-based interferometry, thermal drifts and mechanical imprecision, for example, due to co-alignment errors between optical axes and mechanical axes of rotation can contribute to baseline errors. These errors can be significant at optical and infrared wavelengths but are much less important at radio wavelengths.

Finally, a major difference between ground-based and space-based interferometers is that there are likely to be far fewer telescopes employed in the latter as compared to the former. Hence there will be at most a few closure phases and a closure amplitude available, e.g., for a 4 telescope configuration, there are six baselines (and visibility amplitudes and phases), 4 closure phases (3 independent) and one closure amplitude. However, for planet detection, the strong (essentially) point source from the star allows for multi-wavelength techniques to be used as described above, such that the interferometer is stabilized at $2 \mu\text{m}$ and the planets are detected at $10 \mu\text{m}$. Thus at any given time, there are closure phases at $2 \mu\text{m}$ available to calibrate the closure phases in the $10 \mu\text{m}$ science band, and this can be done essentially continuously, and both for source as well as calibrator. This means that in space based planet detection, both the intrinsic precision and calibration are expected to be much better than can be attained on the ground.

In the next section we describe a possible implementation of a three telescope closure phase nulling interferometer for planet detection.

4. A closure phase nulling interferometer concept

Figure 4 displays a conceptual block diagram for a three telescope nulling interferometer concept that is analogous to ground based interferometers that typically measure three visibilities and a closure phase. In this concept, electric fields, E_1 , E_2 , and E_3 from the three telescopes, with baselines B_{12} , B_{23} , and B_{13} between them, are first incident on ideal 50% beamsplitters, labeled BS, in the diagram. After this, one of the two beams split from each

telescope is passed through an achromatic π phase shifter, and is mixed with a non-phase shifted counterpart from one of the other telescopes. This produces three nulled and three bright outputs. For example, 50% of the light from telescope 1 (blue line) is mixed with 50% of the light from telescope 2 (dashed line), which had previously passed through a π phase shifter, denoted by the purple rectangle in the drawing. The resultant output beams from this second beamsplitter are drawn with the blue dashed lines, and have intensities I_{A1} and I_{A2} as labeled in the figure. The other output beams are I_{B1} , I_{B2} , and I_{C1} , I_{C2} , for baselines B_{23} and B_{13} , respectively.

Following the analysis of Section 1 (e.g. Eqn. (4)), we can write the normalized intensities at the null output ports, as \tilde{I}_{A1} , \tilde{I}_{B1} , \tilde{I}_{C1} , with corresponding bright output intensities, \tilde{I}_{A2} , \tilde{I}_{B2} , \tilde{I}_{C2} . As in Eqn. (4), the null intensities are given by:

$$\tilde{I}_{A1} = 1/2 [1 - |V_{12}| \cos(\phi_{12} + \phi_1 - \phi_2)] \quad (17)$$

$$\tilde{I}_{B1} = 1/2 [1 - |V_{23}| \cos(\phi_{23} + \phi_2 - \phi_3)] \quad (18)$$

$$\tilde{I}_{C1} = 1/2 [1 - |V_{13}| \cos(\phi_{13} + \phi_1 - \phi_3)] \quad (19)$$

Consequently, the system described in Fig. 4 has three null outputs, three bright outputs, and a closure phase.

Figure 5 displays a numerical example for a three telescope system with baselines $B_{12} = 5\text{m}$, $B_{23} = 25\text{m}$, and $B_{13} = 30\text{m}$. We take the same star-planet parameters as the example in the previous section, $I_B = 10^{-6}$, and $I_A = 1 - I_B$, and an angular separation of 0.1 arcsec, the Earth-Sun separation at 10 pc. We can see the substantial difference in null output intensities for the three baselines, B_{12} (red), B_{23} (green), and B_{13} (blue), and the behavior of the closure phase, which has substantial variations with rotation angle. The additional information from the closure phase added to the conventional intensity measurements from the null and bright outputs will improve the detection performance considerably.

5. Discussion

There are many advantages to this type of architecture, and we summarize a few of them in this section. One advantage is due to the non-redundant nature of the baseline configuration. If the telescopes are movable, i.e., on free-flying satellites, the baseline spacing can be varied according to the distance and expected characteristics of the desired sources. With one short and two longer baselines it should be possible to discriminate with more certainty between contributions from the star and planets compared with a non-uniform, asymmetric, or clumpy exozodiacal dust cloud. This is important because the planets are

point sources, while the exozodiacal cloud itself and clumps are extended sources, and most likely will be resolved on the longer baselines.

The characteristic parameters of multiple planets and planetary systems should be more easily deconvolved from the data from this architecture, because the inner planets will be resolved on shorter baselines than the outer ones, so the nulled outputs will vary as a function of baseline rotation angle with much more unique signatures than could be expected from redundant baseline Dual-Chopped Bracewell type architectures. As a result one would expect to have fewer false positive and false negative detections than in these other systems.

The leakage of stellar light into the null outputs will also vary depending on baseline, which could be used to help reduce contamination of the planetary spectrum by the stellar spectrum, and hence extract cleaner planetary spectra for all the planets in a planetary system.

This architecture will also allow for more strategies to deal effectively with non-fundamental noise sources, particularly ones such as pathlength fluctuations, gain variations, and baseline drifts. For the pathlength fluctuations, Danchi et al. (2003) developed a “ratio of wavelengths” technique that allows substantial pathlength fluctuations to be cancelled out of the data, and provides for a cleaner estimation of planet flux as a function of wavelength. Gain variations in the system, such as from mispointing will produce intensity fluctuations at the bright outputs, which could be used in a feedback loop to reduce the variations at the nulled outputs, and thus reduce this type of “common mode” noise source.

Given the reduction in unwanted noise sources and the possible relaxation of dimensional tolerances and precision, it may be possible to reduce substantially the complexity of TPF-I. In particular, it may be possible to simplify or reduce the need for complex metrology systems that may be necessary to ensure adequate baseline stability and knowledge. This is a highly desirable avenue of research as a reduction in complexity of any space system, increases overall system reliability, and reduces cost and risk for the mission.

In summary, our analysis suggests the TPF-I missions could benefit from the closure-phase nulling interferometer system suggested in this paper. Much more detailed analysis, beyond the scope of what is presented here, is necessary to understand the true benefits associated with this new architecture for TPF and Darwin.

This work was supported in part by a grant from NASA Goddard Space Flight Center Director’s Discretionary Fund (DDF).

REFERENCES

Angel, J.R.P., & Woolf, N.J., 1997 *ApJ*, 475, 373.

Barry, R.K., et al. 2005, *Proc. SPIE*, 5905, 311.

Beichman, C.A., Woolf, N., Lindensmith, C. 1999, [Pasadena: Caltech, Jet Propulsion Laboratory], JPL Publication 99-3.

Bracewell, R. 1978, *Nature*, 274, 780.

Bracewell, R., & McPhee, 1979, *Icarus*, 38, 136.

Cornwell, T.J. & Fomalont, E.B. 1999, in *ASP Conf. Series* 180, 187.

Danchi, W.C., Deming, D., Kuchner, M., & Seager, S. 2003, *ApJ*, 597, L57.

Danchi, W.C., et al. 2004, *Proc. SPIE*, 5491, 236.

Hale, D.D., Weiner, J., & Townes, C.H. 2004, *Proc. SPIE*, 5491, 490.

Hyde, T.T., et al. 2004, *Proc. SPIE*, 5491, 553.

Goodman, J.W. 1985, in *Statistical Optics*, [New York: John Wiley & Sons].

Jennison, R. 1958, *MNRAS*, 118, 276.

Leger, A., Mariotti, J.M., Mennesson, B., Ollivier, M., Puget, J.L., Rouan, D., & Schneider, J. 1996, *Icarus*, 12, 249.

Mennesson, B., & Mariotti, J.M., 1997, *Icarus*, 128, 202.

Pearson, T.J., & Readhead, A.C.S. 1984, *ARA&A*, 22, 97.

Perley, R.A. 1999, *ASP Conf. Series*, 180, 275.

Ragland, S., Traub, W.A., Berger, J.-P., Millan-Gabet, R., Monnier, J.D., Pedretti, E., Schloerb, F.P., Carleton, N.P., Hagenauer, P., et al. 2004, *Proc. SPIE*, 5491, 1390.

Thompson, A.R., Moran, J.M., & Swenson, G.W. 2001, 2nd edition, [New York: John Wiley & Sons], p. 73.

Tuthill, P.G., Monnier, J.D., & Danchi, W.C. 1999, *Nature*, 398, 487.

Woolf, N.J., et al. 1998, *Proc. SPIE*, 3350, 683.

Young, J.S., Baldwin, J.E., Boysen, R.C., Haniff, C.A., Lawson, P.R., Mackay, C.D., Pearson, D., Rogers, J., St.-Jacques, D., Warner, P.J., Wilson, D.M.A., Wilson, R.W. 2000, MNRAS, 315, 635.

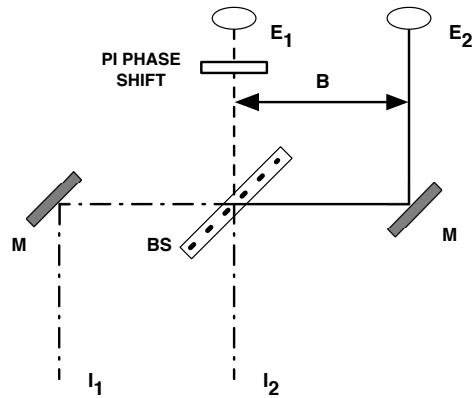


Fig. 1.— Conceptual block diagram of a simplified nulling interferometer.

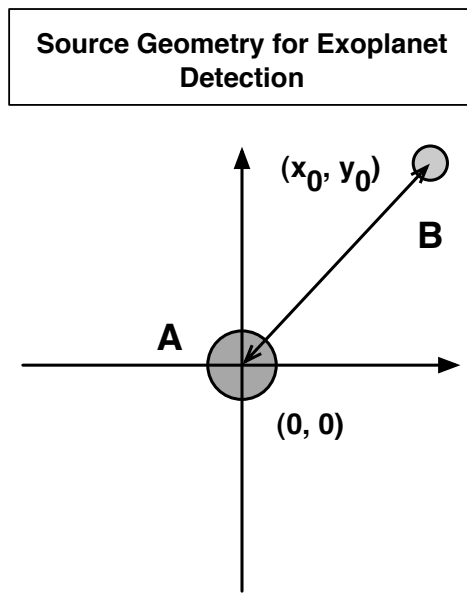


Fig. 2.— Binary geometry used in the discussion.

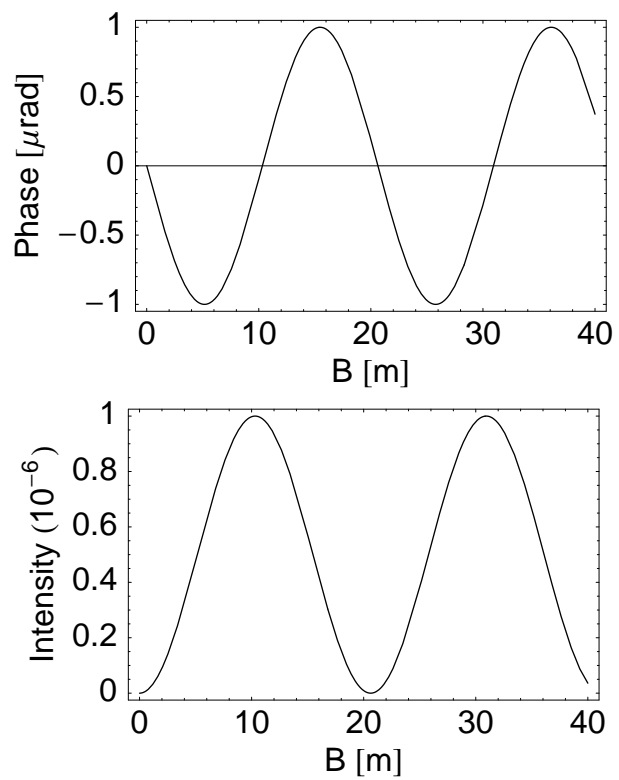


Fig. 3.— (a) Phase in micro-radians for the Earth-Sun system at 10 pc as a function of baseline length in meters. (b) Intensity of null output port as a function of baseline length.

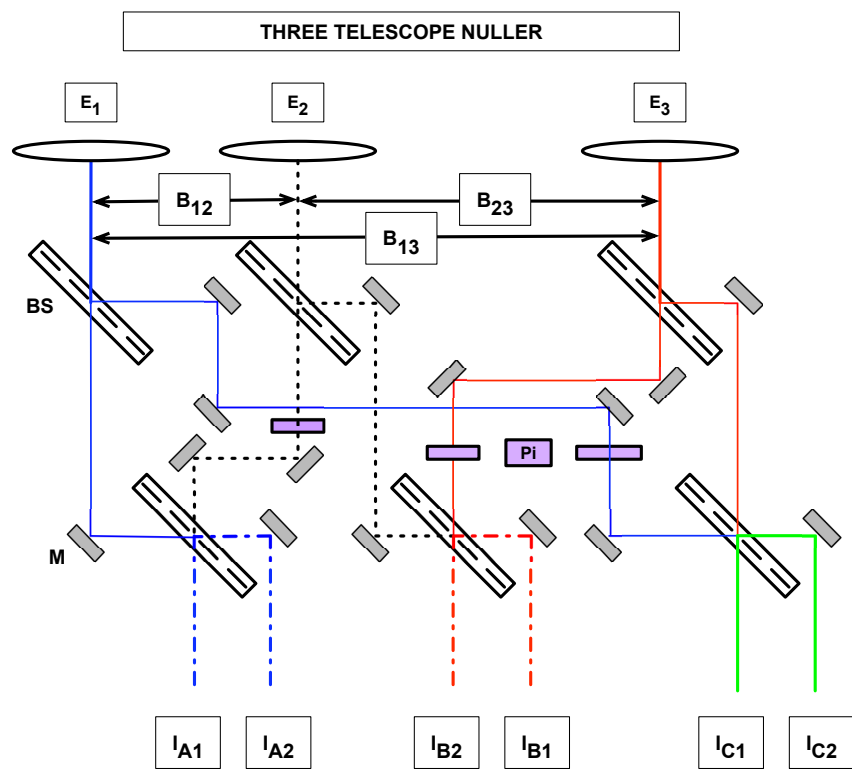


Fig. 4.— Conceptual block diagram of a three-telescope closure-phase nulling interferometer.

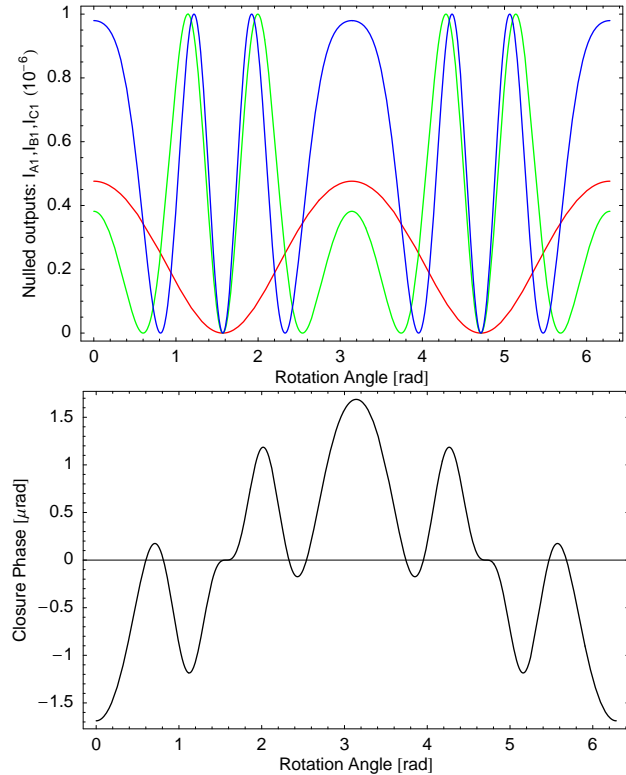


Fig. 5.— (a) Intensities of the three nulled outputs for the Earth-Sun system at 10 pc for a 3 telescope closure phase nulling interferometer with baselines of 5 m (red), 25 m (green), and 30 m (blue) as a function of baseline rotation angle, for an interferometer whose baseline is rotated in a plane perpendicular to the line of sight to the source. (b) Closure phase as a function of rotation angle for parameters in (a) above.